

# MM-Skin: Enhancing Dermatology Vision-Language Model with an Image-Text Dataset Derived from Textbooks

Wenqi Zeng<sup>1</sup>, Yuqi Sun<sup>1</sup>, Chenxi Ma<sup>1</sup>, Weimin Tan<sup>1</sup>, Bo Yan<sup>1</sup>

<sup>1</sup>Shanghai Key Laboratory of Intelligent Information Processing, School of Computer Science, Fudan University, Shanghai, China

## Abstract

Medical vision-language models (VLMs) have shown promise as clinical assistants across various medical fields. However, specialized dermatology VLM capable of delivering professional and detailed diagnostic analysis remains underdeveloped, primarily due to less specialized text descriptions in current dermatology multimodal datasets. To address this issue, we propose MM-Skin, the first large-scale multimodal dermatology dataset that encompasses 3 imaging modalities, including clinical, dermoscopic, and pathological and nearly 10k high-quality image-text pairs collected from professional textbooks. In addition, we generate over 27k diverse, instruction-following vision question answering (VQA) samples (9× the size of current largest dermatology VQA dataset). Leveraging public datasets and MM-Skin, we developed SkinVL, a dermatology-specific VLM designed for precise and nuanced skin disease interpretation. Comprehensive benchmark evaluations of SkinVL on VQA, supervised fine-tuning (SFT) and zero-shot classification tasks across 8 datasets, reveal its exceptional performance for skin diseases in comparison to both general and medical VLM models. The introduction of MM-Skin and SkinVL offers a meaningful contribution to advancing the development of clinical dermatology VLM assistants.

## Keywords

Dermatological Datasets, Vision-Language, Visual Question Answering

## 1 Introduction

Large Vision-Language Models (LVLMs) have shown strong capabilities in visual understanding and natural language generation [2, 14, 16, 32, 38, 54]. In healthcare, several LVLMs [13, 34, 35], such as HuatuoGPT and LLaVA-Med [23, 50], have been developed to assist clinical decision-making. In addition to general medical LVLMs, specialized models targeting specific medical domains have also emerged, such as XrayGPT [43], RepsNet [41], and PathChat [33], predominantly focusing on radiology or pathology.

However, specialized dermatology LVLMs remain largely undeveloped. Recently, SkinGPT-4 [56] was proposed as an innovative solution for interactive dermatology diagnosis. Despite its potential, SkinGPT-4 faces several constraints: 1) Training Datasets. SkinGPT-4’s ability to generate specialized descriptions is limited by the narrow scope of Skincon [11] dataset, which includes only 48 clinical concepts, 1 image modality (clinical), and 3k images. While larger publicly available datasets are used for training, they provide only labels without image descriptions, further restricting the model’s ability to generate detailed responses; 2) Accessibility. Full model weights are not publicly available due to privacy concerns,

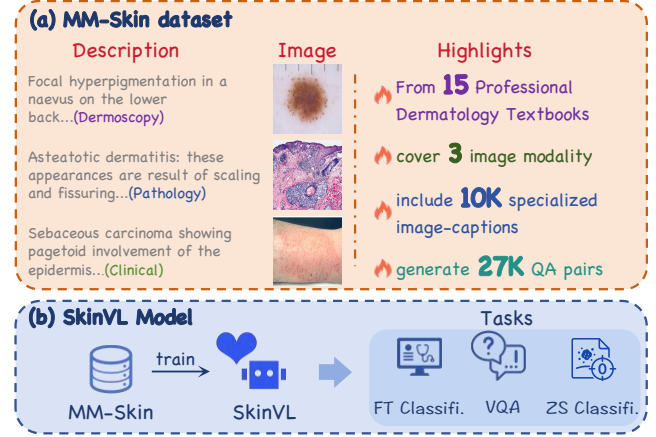


**Figure 1: The proposed MM-Skin dataset and SkinVL model. MM-Skin is the first high-quality dermatology vision-language dataset featuring professional captions, multi-modal images (clinical, dermoscopic, and pathological), and QA pairs. SkinVL, trained on MM-Skin, supports Visual Question Answering (VQA), supervised fine-tuning (SFT), and zero-shot (ZS) classification.**

hindering further development and accessibility; 3) Image Modality. SkinGPT-4 focuses only on clinical and dermoscopic images, excluding pathological images, which limits its comprehensive diagnostic capabilities. Given these challenges, developing a publicly available, specialized dermatology VLM is crucial for advancing the field.

The absence of dermatology-specific LVLMs is primarily due to the scarcity of public, high-quality dermatology image-text datasets, which are essential for generating grounded, interpretable, and instruction-following answers [24]. However, access to dermatology image descriptions is limited. Unlike radiological images, which are typically paired with detailed reports [20, 52], clinical and dermoscopic images often lack written descriptions as part of the examination process, making it difficult to obtain expert descriptions. Additionally, most medical vision question answering (VQA) approaches [5, 25, 27, 36] treat the task as classification or retrieval using predefined answer sets, limiting their ability to handle open-ended clinical questions. Currently, the only public dermatology VQA dataset, DermaVQA [49], is limited in size (3.5k images), modality (only clinical images), and answer quality (sourced from patient consultation websites with variable answer reliability). As a result, current dermatology LVLMs struggle with complex reasoning, highlighting the need for richer visual-language representations.

To address these challenges, we propose **MM-Skin** shown in Figure 1(a), a large-scale, high-quality, multimodal dataset specifically designed for dermatology. MM-Skin consists of nearly 10,000 image-text pairs covering 3 key imaging modalities: clinical photographs, dermoscopy, and pathology. All data are collected from 15 dermatology textbooks authored by experienced dermatologists, and each image is paired with long-form textual descriptions. To further support generative modeling, we leverage large language models (LLMs) to reformat these image-text pairs into over 27,000 instruction-following VQA samples. Compared to existing public dermatology datasets, MM-Skin offers a wealth of QA pairs and more detailed, professional, and diverse descriptions.

We developed **SkinVL** as shown in Figure 1(b), a domain-specific skin vision-language model, using MM-Skin and 9 public skin disease datasets, totaling 171.6k images. We evaluate the model on downstream tasks including VQA, supervised fine-tuning (SFT) and zero-shot diagnosis classification. Furthermore, we benchmark 7 representative LVLMs, including 5 general and 2 medical models, to systematically evaluate their performance. Our results highlight the importance of scalable and grounded medical datasets for improving the reasoning and generalization capabilities of LVLMs in healthcare. Our model has the advantage of generating more detailed, professional responses to a wider variety of questions.

**Our contributions are summarized as follows:**

- We propose MM-Skin, the first large-scale multimodal dermatology dataset with specialized long-text descriptions, including 10k image-text pairs and 27k QA pairs across 3 imaging modalities: clinical, dermoscopic, and pathological.
- We develop SkinVL, the first publicly available dermatology-specific LVLm capable of generating detailed and clinically meaningful responses, tailored for precise and nuanced skin disease interpretation.
- Comprehensive benchmarking of SkinVL on VQA, SFT, and zero-shot diagnosis classification tasks across 8 datasets demonstrates that SkinVL outperforms general and medical VLMs, demonstrating the effectiveness of MM-Skin for dermatology-specific visual understanding.

## 2 Related Work

### 2.1 Existing Medical VQA Datasets

In recent years, an increasing number of datasets have been designed to advance medical VQA research. Table 1 compares existing medical VQA datasets, which are crucial for medical LVLMs. Earlier datasets like VQA-RAD[22], VQA-Med[3], SLAKE[28], and PathVQA[17] are limited by their small size (less than 20k) and their exclusive focus on radiology, which is insufficient for training high-performing models. Large-scale datasets such as PMC-VQA[53] and OmniMedVQA[18] are constructed by generating question-answer pairs with the use of LLMs. Despite the quantity, images in PMC-VQA, 80% of which pertain to radiology, were extracted from online papers, raising concerns about the quality and the diversity. Similarly, QA pairs of OmniMedVQA are derived from classification attributes that are not as descriptive or informative as captions, which may lead to the homogeneity of generated questions. Additionally, all these datasets suffer from limited text length, hindering

their utility for more complex tasks like fine-grained image-text interactions and detailed medical instruction following QAs.

In the field of dermatology, long-text multimodal VQA datasets are notably scarce. Recently, the first public dermatology-specific VQA dataset DermaVQA was developed[49]. However, it is constrained by inaccurate text descriptions, low-quality images collected from a mobile-based telemedicine platform, and a small sample size of around 3k images with a single modality (clinical images of patients), which restricts its broader clinical applications. In contrast, our dataset provides the first dermatology-focused long-text multimodal VQA dataset with nearly 10k high-quality image-text pairs and 27k question-answer pairs across dermoscopy, clinical images, and pathology modalities.

### 2.2 Medical LVLMs

The explosion of LVLMs has significantly advanced medical AI like medical consultation[1, 32] or disease diagnosis[4, 44]. The general medicine domain has witnessed the appearance of models like HuatuoGPT[50], LLaVA-Med[23], Med-Flamingo[35], PeFoMed[30] and Med-PaLM 2[40], while SkinGPT-4 has emerged as a dermatological specialist model[56]. These models primarily use training data sourced from PubMed Central (PMC) and its variants, such as PMC-15M[51], PMC-OA[26], or datasets generated by processing PMC-15M using LLMs, such as LLaVA-Med VQA[23] and PubMedVision[50]. LLaVA-Med, for instance, utilizes medical figure-caption pairs from PMC to scale the dataset and incorporates GPT-4 to transform contextual text into VQA tasks[23]. However, LLaVA-Med still faces limitations in specialized medical fields like dermatology, as its training is primarily based on radiology and pathology, the two most common modalities.

In dermatology, SkinGPT-4[56], an interactive dermatology diagnostic system, was trained on a large collection of public and private dermatology images with diagnostic labels. However, the domain-specific adaptation of SkinGPT-4 relies on an initial training set with only 3K images and 48 clinical concepts (Skincon[11]), limiting its ability to fully capture the diversity and heterogeneity of skin disease characteristics. Furthermore, this simplistic image-concept mapping may restrain the understanding and reasoning of the relationships among medical features displayed in the images. Hence, deploying LVLMs in real-world clinical scenarios is challenging, particularly for a patient’s consultation other than diagnosis, highlighting the urgent need for specialized long-text training datasets in the dermatological domain.

## 3 Methods

### 3.1 MM-Skin Construction

**3.1.1 Data Collection.** We will describe the construction of the MM-Skin dataset, with an overview in Figure 2. A semi-automatic pipeline with five steps was designed to create high-quality image-text pairs across dermoscopic, clinical, and pathology modalities.

**Image-Text Pair Collection:** First, image-text pairs are collected from 15 professional dermatology textbooks. Each image in the pair is ensured to have a resolution of at least  $300 \times 300$  pixels. Following the procedure described in[48], we utilize Adobe API and OCR techniques for raw image and text extraction.

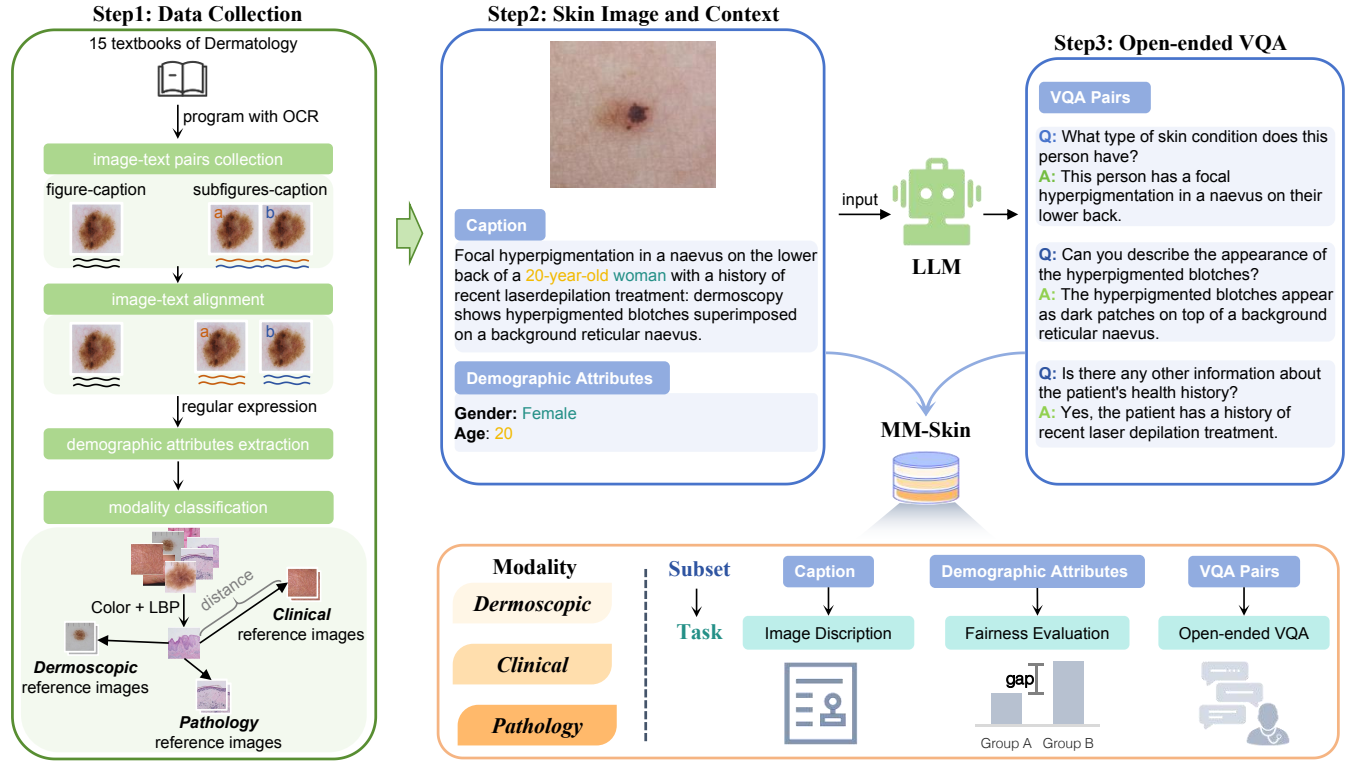


Figure 2: Illustration of the proposed pipeline for constructing MM-Skin, a dataset containing multimodal images, specialized captions, demographic attributes, and QA pairs, supporting multiple downstream tasks.

Table 1: Comparison of public non-dermatology and dermatology medical VQA datasets with our proposed MM-Skin dataset.

Domain	Dataset	Modality	# images	# QA pairs	Answer Length	# image-text pairs	# demographic attributes
Non-Dermatology	PathVQA	Pathology	5K	32K	2.5	×	×
	VQA-RAD	Radiology	0.3K	3.5K	1.6	×	×
	SLAKE	Radiology	0.7K	14K	-	×	×
	VQA-Med	Radiology	5K	5K	1(74%);2(2%); 3(20%);4(4%)	✓	×
	PMC-VQA	Mixture(80%Radiology)	149K	227K	-	×	×
	OmniMedVQA	Mixture	118K	128K	-	×	×
Dermatology	DermaVQA	Clinical	3.4K	1.5K	11.9(66%); 94.6(34%)	×	×
	MM-Skin	Clinical; Pathology; Dermoscopy	11K	27K	21.67	✓	✓

**Image-Text Alignment:** Some extracted images and texts do not align perfectly, as sub-figures share a single caption. We use regular expression matching to separate captions and align the image-text pairs accurately.

**Modality Classification:** Given that the images in the textbooks encompass multiple modalities, we categorize the images into dermoscopic, clinical, and pathology types. This classification is based on extracted features, such as the color histogram and local binary pattern (LBP). Let the extracted features for an image be denoted as  $\mathbf{x}$ , which consists of the color histogram and LBP features. To classify an image, we extract features  $\mathbf{x}_{\text{ref}_i}$  from reference images and construct a feature library. The test image  $\mathbf{x}_{\text{test}}$  is compared to each reference using a distance metric, and the image is assigned to the category corresponding to the reference image with the smallest

distance:

$$d(\mathbf{x}_{\text{test}}, \mathbf{x}_{\text{ref}_i}) = \|\mathbf{x}_{\text{test}} - \mathbf{x}_{\text{ref}_i}\|$$

$$\hat{y} = \arg \min_i (d(\mathbf{x}_{\text{test}}, \mathbf{x}_{\text{ref}_i}))$$

Finally, the classification is verified manually to ensure accuracy. **Text Cleaning and Demographic Attributes Extraction:** Demographic attributes such as age and gender are extracted by matching relevant keywords in captions using regular expression techniques. **Filtering and Processing:** Threads with images of genitalia, identifiable features (e.g., special tattoos), image annotations (e.g., drawn arrows), or full-face photos were removed. Detailed annotation guidelines are included in our data release.

**3.1.2 VQA Generation.** Although there are many Medical VQA datasets[17, 22, 28] available, they all have two significant drawbacks that limit their practicality: (1) In the field of dermatology,

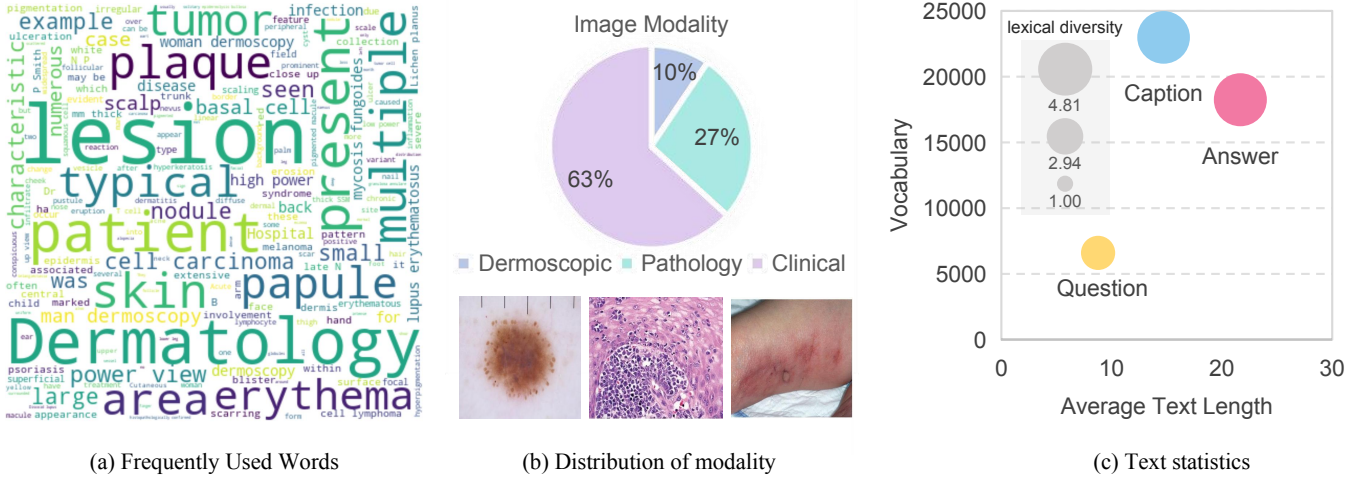


**Figure 3: Statistical overview of the MM-Skin dataset. (a) Word cloud of caption texts, illustrating the diversity of dermatological terms. (b) Distribution of the three imaging modalities with representative examples. (c) Comparison of average text length, vocabulary size, and lexical diversity (Herdan’s C) for questions, answers, and captions.**

open-source datasets for detailed question-and-answer interactions are notably scarce, especially those with professionally accurate text descriptions and large-scale data; and (2) Many current VQA datasets consist of simple closed-ended multiple-choice questions, while open-ended question-answering typically provides brief responses to straightforward queries, such as diagnostic questions, rather than generating long-form answers to diverse and complex inquiries. These limitations significantly restrict the flexibility and comprehensiveness of the datasets in addressing a broader range of user questions. Therefore, these issues highlight the need for a more extensive, long-text dataset like MM-Skin.

Large models are increasingly used to generate high-quality data, addressing data scarcity[23, 29, 50]. As shown in Figure 2, we prepare to generate our VQA dataset after extracting image-caption pairs from professional dermatology textbooks. Here, we employ Llama-3.1[45] as a generator to curate diverse instruction-following data with multi-round conversations about the provided skin images. Specifically, given an image caption, we design instructions in a prompt that asks the LLM to generate multi-round questions and answers in a tone as if it could “see” the image. Moreover, we also design specific rules (e.g., ensuring that no information not explicitly stated in the caption or context is introduced) to maintain the quality of the generated VQAs. The multi-round questions and answers are generated as follows:

$$\{q_1, a_1, q_2, a_2, \dots, q_n, a_n\} = \text{LLM}(I, X)$$

where  $I$  is the image,  $X$  is the corresponding image description, and  $\{q_1, a_1, q_2, a_2, \dots, q_n, a_n\}$  represents the sequence of multi-round questions and answers generated by the LLM. See Appendix B for the prompt examples.

### 3.2 MM-Skin Statistics

The current version of the MM-Skin dataset includes 11,039 images, of which 1,039 are dermoscopic, 3,016 are pathology, and 6,984 are

**Table 2: Statistics of Image Type in MM-Skin.**

Image Type	# Images	# Image-text pairs	# QA pairs	# Gender	# Age
Dermoscopy	1039	969	2865	487	475
Pathology	3016	2697	7834	14	6
Clinical	6984	5703	16713	274	133
Overall	11039	9369	27412	775	614

clinical. The MM-Skin dataset can be divided into three subsets: MM-Skin-C (MM-Skin-Caption), MM-Skin-O (MM-Skin-OpenEnded), and MM-Skin-D (MM-Skin-Demographic), each corresponding to a specific downstream task. MM-Skin-C is used for image description, MM-Skin-O for open-ended VQA, and MM-Skin-D for fairness evaluation, which assesses whether the model performs equally well across different demographic groups (e.g., male and female patients). The number of corresponding professional text descriptions, QA pairs, and demographic sample information for each image is shown in Table 2. A detailed statistical analysis of the data is provided in Figure 3, focusing on aspects such as frequently used words, text length, and vocabulary size.

**Frequently Used Words:** To probe the diversity and coverage of image classes in MM-Skin, we generated a word cloud of the captions, shown in Figure 3(a). Since the MM-Skin dataset is built based on comprehensive skin disease textbooks, it covers a wide range of disease categories, such as plaque, tumor papule, carcinoma, and erythema. Additionally, it includes words related to patient identity features, such as “child”.

**Modality Distribution:** MM-Skin includes images from three skin imaging modalities. As shown in Figure 3(b), clinical images constitute the majority (63%), while dermoscopic images are the least represented (10%). This diverse modality distribution offers broad coverage of skin disease types, which is essential for evaluating multimodal models in dermatology.



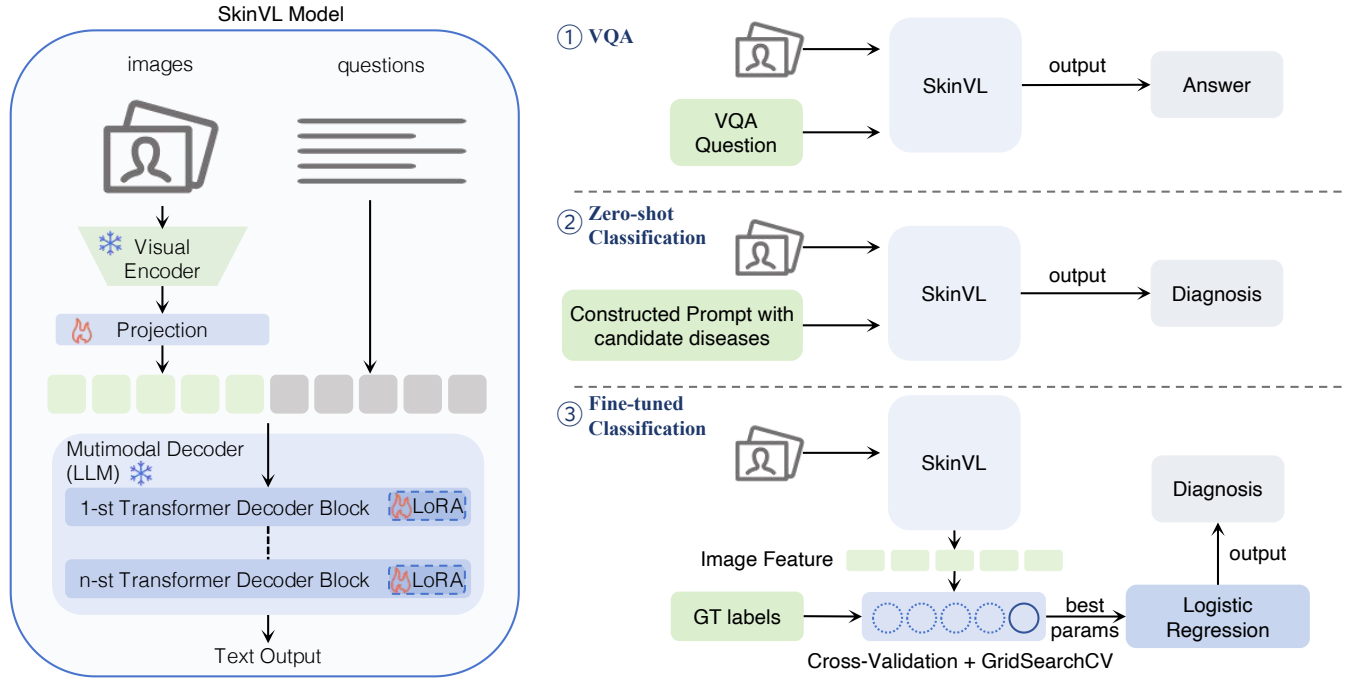


**Figure 4: Overview of the SkinVL architecture, where the CLIP-ViT-L/14 visual encoder and language model decoder (LLaVA-Med) remain frozen, with only the visual projection layer and LoRA modules being updated. The figure also illustrates the evaluation procedures for visual question answering, supervised fine-tuning classification, and zero-shot classification.**

**Text Length and Vocabulary Size:** MM-Skin contains diverse textual descriptions, including disease diagnoses, lesion characteristics (e.g., color, shape, appearance), clinical manifestations, and post-treatment efficacy information. Figure 3(c) displays the average text length, average vocabulary size, and lexical diversity across the three subsets. The average vocabulary size represents the total number of unique words across all the texts in the dataset, and lexical diversity is measured using Herdan’s  $C$ , given by  $C = \frac{|V|}{\log N}$ , where  $|V|$  is the number of unique words and  $N$  is the total number of words in the text. This metric helps assess the richness and diversity of the vocabulary used in the dataset.

### 3.3 SkinVL Model

**3.3.1 Fine-Tuned on MM-Skin.** To validate the effectiveness of the MM-Skin dataset, specifically the auto-generated training set, we fine-tuned the LLaVA-Medv1-7B model[23] on dermatology-specific multimodal datasets. We employed Low-Rank Adaptation (LoRA) instruction tuning to apply efficient parameter tuning on the LLaVA-Med backbone without retraining the entire model. This setup focuses on optimizing the parameters in the visual projector and the LoRA adapters, while keeping the vision encoder and the language model decoder frozen. All models are evaluated on three tasks: VQA, supervised fine-tuned diagnosis classification, and zero-shot diagnosis classification. The overall model structure is shown in Figure 4. To investigate the impact of training data sources, we provide three variants of SkinVL, each trained on different datasets to assess how textual diversity and data quality affect performance:

**SkinVL-MM:** This model variant was trained solely on the MM-Skin dataset, which contains high-quality image-text pairs across clinical, dermoscopic, and pathological modalities, with a total of 21.8k images. Each image is paired with long specialized descriptions covering a comprehensive range of dermatological diseases.

**SkinVL-Pub:** Trained on the training sets of 9 public skin disease classification datasets, including DDI[10], HIBA[39], BCN20000[9], Fitzpatrick17k[15], ISIC 2019[8, 46], SCIN[47], PAD-UFES-20[37], Patch16[21], and MSKCC[7]. The combined training set consists of 149k images in total. They contain diagnostic labels but do not provide QA-format supervision. To standardize with MM-Skin, we reformulated the diagnosis labels into question-answer pairs (e.g., “What is the diagnosis?” → “Melanoma”).

**SkinVL-PubMM:** This model was fine-tuned on a combined dataset of MM-Skin and reformatted public datasets, totaling 171.6k images, leveraging both specialized dermatology knowledge and a broader range of diagnostic labels.

**3.3.2 Downstream Tasks.** The models were evaluated across 3 experimental tasks: VQA, supervised fine-tuning (SFT) classification, and zero-shot classification. The overall methodologies for these tasks are shown on the right side of Figure 4.

**Visual Question Answering (VQA).** The model was provided with unseen images and related questions, allowing it to generate responses. The goal was to test its ability to generate accurate and contextually relevant answers based on visual content and assess how well it generalizes to new queries.

**Supervised Fine-tuned Classification.** To assess the generalization ability of visual representations, we extract image features from vision encoder and train a logistic regression classifier on downstream datasets using the corresponding ground-truth diagnostic labels. For each input image  $I$ , the visual feature is computed as:

$$f(I) = P_{\text{mm}}(E_{\text{vision}}(I)) \in \mathbb{R}^d$$

where  $E_{\text{vision}}(\cdot)$  is the visual encoder and  $P_{\text{mm}}(\cdot)$  is the multimodal projection layer. The logistic regression classifier is trained as:

$$\hat{y} = \text{softmax}(W^T f(I) + b)$$

where  $W \in \mathbb{R}^{d \times C}$ ,  $b \in \mathbb{R}^C$ , and  $C$  is the number of disease categories. Hyperparameters are optimized using grid search over the regularization parameter  $C \in \{10^{-5}, \dots, 10^1\}$ . We perform five-fold cross-validation using ROC-AUC as the selection metric. After finding the best hyperparameters, the classifier is retrained on the full training set and evaluated on validation and test splits.

**Zero-shot Classification.** To assess the model’s diagnostic reasoning ability in a zero-shot setting, we designed a classification task without any training on the downstream data. Given an input image  $I$ , we constructed prompts  $Q_C$  containing a list of candidate disease categories  $C = \{c_1, c_2, \dots, c_n\}$  and paired these with images, as shown in Figure 5. The prompt  $Q_C$  and image  $I$  are jointly input into the model, which generates a textual answer  $\hat{A}$ . The prediction is then matched to one of the candidates in  $C$ . This setup mimics real-world clinical applications where the model must infer diagnostic labels in the absence of task-specific supervision. It also evaluates the model’s capacity to perform grounded medical reasoning across previously unseen categories and datasets.

```
<Ori System Prompt><STOP>
Human:<image>\n $\mathbf{x}_{\text{question}}$ : This is a skin
lesion image. From the following categories:
{possible_diseases}, which one is the
diagnosis? <STOP>
Assistant: <answer> $\mathbf{x}_{\text{answer}}$ <STOP>
```

Figure 5: Input format for zero-shot classification.

## 4 Experiment

### 4.1 Experimental Setup

**Evaluation Data.** We evaluated the model using test sets from the MM-Skin dataset and public datasets covering all three imaging modalities. We followed the official test set splits when available; otherwise, datasets were split 8:2 for training and testing.

- VQA: Evaluated on the MM-Skin test set, with 5.5k images.
- SFT classification: Evaluated on test sets from 8 public skin datasets across dermoscopic, clinical, and pathological modalities, with a total of 43k images. Specifically, the datasets include dermoscopic images from HAM10000 [46], ISIC 2019 [8], and HIBA [39]; clinical images from DDI [10], Fitzpatrick17k [15], and PAD-UFES-20 [37]; and pathological images from Patch16 [21].

- Zero-shot classification: we evaluated the model on test sets from Patch16 and additionally included HAM10000 [46] and Dermnet [12], which were not seen during training, to test the model’s ability to generalize to unseen data under zero-shot conditions, totaling 33.5k images.

**LVLMS Benchmarks.** SkinGPT-4 was not included in our comparison due to the unavailability of its full model weights caused by privacy restrictions, yet we performed a qualitative comparison using its released partial weights (step-1) in the case study. Besides fine-tuning a task-oriented model, we evaluated 7 LVLMS, including 5 general-purpose models (doubao-1-5-vision-pro-32k, Gemini Flash2.0[42], InternVL 2.5-8B[6], Qwen2.5-VL-7B[2], LLaVA-v1.6-7B[31]) and 2 medical-domain models (LLaVA-Med-7B[23], HuatuoGPT-7B[50]), to assess their capabilities in skin-related tasks.

**Training Details.** We fine-tune both the visual projection layers and LLM components of LLaVA-Med-v1.5 using LoRA, starting from the original model weights. Training is done on eight NVIDIA 3090 GPUs with a batch size of 16 per device. LoRA is applied with a rank of 128 and alpha of 64. The learning rate is  $5e-5$  with cosine decay, and gradient checkpointing is used to optimize memory. We also employ bf16 precision and Fully Sharded Data Parallel (FSDP) for better speed and scalability, with Deepspeed managing the training process and periodic model checkpoints.

**Evaluation Metrics.** We assessed the VQA models using BLEU-4, METEOR, ROUGE-L, BERTScore, and Recall to evaluate the linguistic accuracy and relevance of their responses. For classification tasks, we employed Accuracy, Precision, and Balanced Accuracy (BACC) to measure the models’ effectiveness in correctly identifying disease types across various modalities. These metrics provided a comprehensive evaluation of model performance.

### 4.2 Evaluation on Visual Question Answering

To ensure a fair comparison, all evaluated models, with the exception of doubao-1-5-vision-pro and Gemini Flash2.0, are based on 7B-LLMs. Specifically, LLaVA-v1.6 is based on Vicuna-7B-v1.5 [55], LLaVA-Med-v1.5 utilizes Mistral-7B-Instruct-v0.2[19], and HuatuoGPT integrates the LLaVA-1.5 model architecture with LLaMA-3-8B[50]. The configurations of all models were set according to their respective open-source codes. The results of these models are summarized in Table 3, with the first five rows presenting the performance of general LVLMS, the next two rows representing medical LVLMS, and the final three rows showing the results of our fine-tuned version of LLaVA-Med based on different training sets.

Most general LVLMS perform poorly on MM-Skin. For instance, doubao-1-5-vision-pro-32k achieves only a Bleu-4 score of 2.16 in the pathology modality, reflecting its inability to generate relevant responses. LLaVA-v1.6-7B shows better recall but still scores low in Bleu-4 (2.14), indicating limited accuracy. Specialized models like LLaVA-Med-7B and HuatuoGPT-7B perform better, with LLaVA-Med-7B achieving 7.70 in Bleu-4 for pathology, and HuatuoGPT-7B scoring 4.42. The higher recall of HuatuoGPT-7B suggests a stronger understanding of medical images, highlighting the benefits of specialized training. The fine-tuned SkinVL-MM model, trained on MM-Skin, shows substantial improvement, achieving a Bleu-4 of 22.04 in pathology. It improves by nearly 10% in Bleu-4

**Table 3: VQA Performance of representative general LVLMs, medical LVLMs, and our SkinVL model on MM-Skin dataset.**

Methods	Pathology					Clinical					Dermoscopy				
	Bleu-4	Meteor	Rouge-l	BertScore	recall	Bleu-4	Meteor	Rouge-l	BertScore	recall	Bleu-4	Meteor	Rouge-l	BertScore	recall
doubao-1.5-vision-pro-32k	2.16	22.45	18.59	56.20	35.00	2.96	24.53	20.23	58.01	36.58	2.61	24.03	19.58	57.76	36.89
Gemini Flash2.0	3.66	19.25	17.93	53.78	26.97	3.69	19.30	18.17	54.80	26.38	3.87	22.88	19.33	56.35	31.27
InternVL 2.5-8B	3.22	23.96	20.68	56.22	37.27	3.67	25.22	22.45	58.27	37.44	3.50	25.81	22.56	58.06	38.90
Qwen2.5-VL-7B	1.97	22.69	16.88	52.50	42.70	2.37	24.31	17.89	54.65	44.81	1.89	22.66	16.26	53.25	47.47
LLaVA-v1.6-7B	2.14	22.92	17.60	53.99	47.25	2.62	24.91	20.04	56.19	46.83	2.32	23.60	19.11	55.07	46.25
LLaVA-Med-7B	7.70	32.24	32.03	63.57	43.67	7.07	32.23	31.88	64.31	42.92	8.88	33.74	34.83	66.60	41.82
HuatuoGPT-7B	4.42	29.03	21.99	58.42	46.31	4.14	29.78	21.69	58.69	47.15	4.01	29.21	21.42	58.49	49.92
SkinVL-MM	<b>22.04</b>	<b>42.70</b>	<b>44.09</b>	<b>70.59</b>	<b>48.20</b>	<b>23.39</b>	<b>43.19</b>	<b>44.32</b>	<b>71.47</b>	<b>47.66</b>	<b>21.61</b>	<b>42.76</b>	<b>44.70</b>	<b>71.34</b>	<b>47.51</b>
SkinVL-Pub	8.08	31.85	31.61	62.24	43.89	6.94	31.48	30.39	62.37	43.66	6.60	29.99	29.53	60.94	43.64
SkinVL-PubMM	<u>16.56</u>	<u>41.64</u>	<u>39.66</u>	<u>68.27</u>	<u>51.29</u>	<u>16.29</u>	<u>41.66</u>	<u>38.87</u>	<u>68.55</u>	<u>50.50</u>	<u>13.48</u>	<u>40.24</u>	<u>37.20</u>	<u>66.89</u>	<u>52.26</u>

**Table 4: SFT Classification accuracy and recall of different models on skin disease datasets across three imaging modalities.**

Methods	Patch16		PAD-UFES-20		ISIC 2019		HIBA		HAM10000		Fitzpatrick		Dermnet		DDI	
	ACC	Recall	ACC	Recall	ACC	Recall	ACC	Recall	ACC	Recall	ACC	Recall	ACC	Recall	ACC	Recall
LLaVA-med	<u>95.37</u>	94.27	<u>73.48</u>	<u>62.42</u>	75.93	56.77	80.43	80.34	78.42	<u>62.13</u>	82.90	64.56	56.77	52.66	<b>84.09</b>	72.96
SkinVL-Pub	95.23	94.15	73.48	61.17	76.33	58.10	81.35	81.14	<b>79.29</b>	60.19	83.18	67.33	<b>57.62</b>	<b>53.88</b>	<b>84.09</b>	<b>74.88</b>
SkinVL-MM	95.27	<b>94.47</b>	71.96	60.96	<u>76.34</u>	<b>58.21</b>	79.20	79.11	<u>79.15</u>	61.54	<b>83.43</b>	<b>67.58</b>	<u>56.95</u>	52.42	<u>83.33</u>	<u>74.37</u>
SkinVL-PubMM	<b>95.63</b>	<u>94.43</u>	<b>75.22</b>	<b>63.99</b>	<b>76.38</b>	57.33	<b>81.65</b>	<b>81.58</b>	78.95	<b>62.58</b>	82.56	65.92	56.87	<u>52.80</u>	82.58	71.94

compared to InternVL 2.5-8B, the best general model for dermoscopic images, demonstrating the effectiveness of domain-specific fine-tuning. SkinVL-MM also excels in contextual relevance, with BertScores exceeding 70 across all modalities, outperforming both general and medical models. While SkinVL-MM trained solely on MM-Skin excels in natural language metrics, combining public data with MM-Skin (SkinVL-PubMM) enhances recall across all modalities. Dermoscopic images show the highest recall, likely due to their higher image quality, emphasizing the importance of image quality in model performance.

### 4.3 Evaluation on SFT classification


To assess the generalization ability of our fine-tuned models beyond the VQA task, we conducted a transfer evaluation on downstream classification. Specifically, we extracted image features from the trained multimodal models and trained a logistic regression classifier using the corresponding ground-truth diagnostic labels. This approach allows us to assess whether the visual representations learned under VQA-style supervision contain sufficient semantic information for skin disease classification, even without direct exposure to diagnostic labels. The evaluation was performed on eight publicly available skin disease datasets, covering three imaging modalities: pathology (Patch16), dermoscopy (ISIC 2019, HIBA, HAM10000), and clinical photography (PAD-UFES-20, Fitzpatrick, Dermnet, DDI). For datasets with official train-validation-test splits, we followed the original partitions. Otherwise, we adopted a 6:2:2 split. For Patch16, we simulated a low-resource setting by using only 10% of the available training and validation data.

As shown in Table 4, the model trained on both MM-Skin and public diagnostic datasets (SkinVL-PubMM) demonstrated the best overall performance, particularly on non-clinical images. It achieved the highest accuracy on Patch16 (95.63%) and HIBA (81.65%), and top recall on ISIC 2019 (57.33%) and HAM10000 (62.58%). Notably,

SkinVL-PubMM surpassed SkinVL-Pub by +1.74% on PAD-UFES-20 and by +0.32% on ISIC 2019, highlighting the benefit of incorporating MM-Skin. Meanwhile, SkinVL-Pub marginally outperformed other models on clinical datasets, achieving the best performance on Dermnet (57.62% ACC) and DDI (84.09% ACC / 74.88% Recall). These trends suggest that MM-Skin enhances feature learning for structured imaging modalities, while public datasets may better support generalization to more variable clinical photographs. Interestingly, the model trained exclusively on MM-Skin (SkinVL-MM), without access to any diagnostic labels during training, still achieved competitive results. Despite being optimized only for VQA using image-text supervision, it attained 76.34% accuracy on ISIC 2019, 83.43% on Fitzpatrick, and 79.15% on HAM10000. Moreover, its recall on Patch16 (94.47%) was nearly identical to that of SkinVL-PubMM (94.43%), with only a 0.04% difference. These results demonstrate that MM-Skin fosters the learning of transferable visual representations, making it a valuable resource not only for VQA tasks but also for broader applications in medical image understanding.

**Table 5: Zero-shot classification performance of representative LVLMs and SkinVL model.**

Methods	Patch16		PAD-UFES-20		HAM10000	
	ACC	precision	ACC	precision	ACC	precision
Qwen2.5-VL-7B	66.29	72.77	<b>45.00</b>	<u>36.52</u>	<u>39.58</u>	<u>26.13</u>
InternVL 2.5-8B	60.97	43.00	32.83	21.76	30.97	17.02
LLaVA-1.6	60.02	23.03	20.00	17.32	3.18	4.91
LLaVA-Med-7B	<u>68.55</u>	<u>82.83</u>	32.39	7.76	5.49	1.43
HuatuoGPT-7B	47.65	39.54	<u>37.17</u>	29.07	19.79	18.65
SkinVL-MM	42.60	24.08	15.00	6.03	3.51	1.51
SkinVL-Pub	68.44	<u>84.22</u>	31.96	21.78	32.56	29.14
SkinVL-PubMM	<b>82.34</b>	<b>86.65</b>	35.65	<b>41.88</b>	<b>51.29</b>	<b>37.37</b>

	Q: Are there any other features in the image that suggest dysplastic nevus syndrome?
	GT: Yes, the presence of <b>numerous atypical nevi</b> is one of the key characteristics of dysplastic nevus syndrome. Additionally, some individuals may also have a <b>family history of melanoma</b> or a personal <b>history of sunburns or excessive exposure to UV radiation</b> .
Qwen2.5-VL	The image shows a person's abdomen with <b>multiple brown spots</b> , which could be indicative of various skin conditions.
LLaVA-Med	Yes, there are additional features in the image that suggest dysplastic nevus syndrome. These include <b>multiple brown macules and a brown macule with a central depression</b> . These features are consistent with the skin manifestations of dysplastic nevus syndrome.
SkinGPT-4*	Permanent and <b>Brown</b> (Hyperpigmented).
SkinVL-PubMM	Yes, there are several other features in the image that suggest dysplastic nevus syndrome. These include the presence of <b>multiple nevi, some of which are atypical</b> , and the presence of a <b>family history of melanoma</b> . Additionally, the patient has a <b>history of sun exposure</b> and has had previous skin cancers removed.

\* SkinGPT-4 results are based on released step-1 weights; full model weights are unavailable due to privacy concerns.

**Figure 6: Qualitative comparison of medical visual question answering on diverse LVLMs using MM-Skin.**

#### 4.4 Evaluation on Zero-shot classification

To evaluate the generalization capabilities of various models in a more practical setting, we conducted a zero-shot classification task. In this scenario, models are required to make predictions without seeing any task-specific labeled training data. This setting closely reflects real-world deployment situations, where the model must infer the correct diagnosis from previously unseen cases. Evaluating zero-shot performance is thus essential for understanding the transferability and robustness of LVLMs. We performed this evaluation on three downstream datasets, each representing a different imaging modality: Patch16 (pathology), PAD-UFES-20 (clinical photography), and HAM10000 (dermoscopy). For each test image, we constructed a query containing all possible diagnosis candidates from the corresponding dataset and prompted the LVLM to select the most likely answer. We compared three general-purpose LVLMs, two medical-specific LVLMs, and three fine-tuned models based on our MM-Skin framework. The results are presented in Table 5

Among all models, SkinVL-PubMM consistently achieved the best performance across datasets. On Patch16, it reached 82.34% accuracy, outperforming LLaVA-Med by +13.79%, and achieved the highest overall precision (86.65%). On dermoscopic data (HAM10000), it remained the only model exceeding 50% accuracy, while others lagged behind, highlighting the effectiveness of combining MM-Skin with public data during fine-tuning. SkinVL-Pub also performed well, with 68.44% accuracy on Patch16, demonstrating the utility of public diagnostic data alone. In contrast, SkinVL-MM, which lacked diagnostic label supervision, struggled in the zero-shot setting, underscoring the importance of explicit label exposure. Among general-purpose models, Qwen2.5-VL-7B stood out with 66.29% on Patch16, occasionally surpassing medical LVLMs. However, models like LLaVA-1.6 exhibited near-zero performance on HAM10000 (3.18%), revealing the limitations of general LVLMs in specialized tasks. Overall, results demonstrate that fine-tuning with domain-specific multimodal data—particularly the combination of MM-Skin and public datasets—substantially enhances zero-shot

classification, offering a practical path toward deploying LVLMs in real-world medical scenarios.

#### 4.5 Case Study

Figure 6 presents a case comparing model responses to a query about dysplastic nevus syndrome. While Qwen2.5-VL provides a basic description and LLaVA-Med identifies some relevant features, SkinGPT-4, based on released available step-1 weights, uses simple terms and lacks the ability to adapt to diverse queries. In contrast, SkinVL-PubMM delivers a more comprehensive and accurate response, recognizing key visual features and integrating patient history, such as family history of melanoma and sun exposure. This demonstrates the value of fine-tuning with both MM-Skin and publicly available datasets to generate clinically grounded responses. Further case studies are available in the supplementary materials.

### 5 Conclusion

In this paper, we propose MM-Skin, the first open-access image-text dermatology dataset with 3 imaging modalities, and SkinVL, a specialized dermatology vision-language model. Our dataset improves model performance by providing high-quality, diverse image-text pairs, which play a pivotal role in advancing dermatology LVLMs. Further research into next-generation medical LVLMs with better reasoning capabilities will benefit from the improvement in the generation of detailed responses. We hope MM-Skin will contribute to the advancement of interactive AI systems in dermatology.



## References

- [1] Asma Alkhalidi, Raneem Alnajim, Layan Alabdullatef, Rawan Alyahya, Jun Chen, Deyao Zhu, Ahmed Alsinan, and Mohamed Elhoseiny. 2024. Minigpt-med: Large language model as a general interface for radiology diagnosis. *arXiv preprint arXiv:2407.04106* (2024).
- [2] Jinze Bai, Shuai Bai, Shusheng Yang, Shijie Wang, Sinan Tan, Peng Wang, Junyang Lin, Chang Zhou, and Mingguang He. 2023. Qwen-VL: A Versatile Vision-Language Model for Understanding, Localization, Text Reading, and Beyond. arXiv:2308.12966 [cs.CV] <https://arxiv.org/abs/2308.12966>
- [3] Asma Ben Abacha, Mourad Sarrouti, Dina Demner-Fushman, Sadid A Hasan, and Henning Müller. 2021. Overview of the vqa-med task at imageclef 2021: Visual question answering and generation in the medical domain. In *Proceedings of the CLEF 2021 Conference and Labs of the Evaluation Forum-working notes*. 21-24 September 2021.
- [4] Xiaolan Chen, Ziwei Zhao, Weiye Zhang, Pusheng Xu, Le Gao, Mingpu Xu, Yue Wu, Yinwen Li, Danli Shi, and Mingguang He. 2024. Eyegpt: Ophthalmic assistant with large language models. *arXiv preprint arXiv:2403.00840* (2024).
- [5] Zhihong Chen, Yuhao Du, Jinpeng Hu, Yang Liu, Guanbin Li, Xiang Wan, and Tsung-Hui Chang. 2022. Multi-modal masked autoencoders for medical vision-and-language pre-training. In *International Conference on Medical Image Computing and Computer-Assisted Intervention*. Springer, 679–689.
- [6] Zhe Chen, Weiyun Wang, Yue Cao, Yangzhou Liu, Zhangwei Gao, Erfei Cui, Jinguo Zhu, Shenglong Ye, Hao Tian, Zhaoyang Liu, et al. 2024. Expanding performance boundaries of open-source multimodal models with model, data, and test-time scaling. *arXiv preprint arXiv:2412.05271* (2024).
- [7] Noel Codella, Veronica Rotemberg, Philipp Tschandl, M Emre Celebi, Stephen Dusza, David Gutman, Brian Helba, Aadi Kallou, Konstantinos Liopyris, Michael Marchetti, et al. 2019. Skin lesion analysis toward melanoma detection 2018: A challenge hosted by the international skin imaging collaboration (isic). *arXiv preprint arXiv:1902.03368* (2019).
- [8] Noel CF Codella, David Gutman, M Emre Celebi, Brian Helba, Michael A Marchetti, Stephen W Dusza, Aadi Kallou, Konstantinos Liopyris, Nabin Mishra, Harald Kittler, et al. 2018. Skin lesion analysis toward melanoma detection: A challenge at the 2017 international symposium on biomedical imaging (isbi), hosted by the international skin imaging collaboration (isic). In *2018 IEEE 15th international symposium on biomedical imaging (ISBI 2018)*. IEEE, 168–172.
- [9] Marc Combalia, Noel CF Codella, Veronica Rotemberg, Brian Helba, Veronica Vilaplana, Ofer Reiter, Cristina Carrera, Alicia Barreiro, Allan C Halpern, Susana Puig, et al. 2019. Bcn20000: Dermoscopic lesions in the wild. *arXiv preprint arXiv:1908.02288* (2019).
- [10] Roxana Daneshjou, Kailas Vodrahalli, Roberto A Novoa, Melissa Jenkins, Weixin Liang, Veronica Rotemberg, Justin Ko, Susan M Swetter, Elizabeth E Bailey, Olivier Gevaert, et al. 2022. Disparities in dermatology AI performance on a diverse, curated clinical image set. *Science advances* 8, 31 (2022), eabq6147.
- [11] Roxana Daneshjou, Mert Yuksekgonul, Zhuo Ran Cai, Roberto Novoa, and James Y Zou. 2022. Skincon: A skin disease dataset densely annotated by domain experts for fine-grained debugging and analysis. *Advances in Neural Information Processing Systems* 35 (2022), 18157–18167.
- [12] DermNet. [n. d.]. *Dermnet*. <https://dermnet.com/>
- [13] Sedigheh Eslami, Christoph Meinel, and Gerard De Melo. 2023. Pubmedclip: How much does clip benefit visual question answering in the medical domain?. In *Findings of the Association for Computational Linguistics: EACL 2023*. 1181–1193.
- [14] Yujie Feng, Zexin Lu, Bo Liu, Liming Zhan, and Xiao-Ming Wu. 2023. Towards LLM-driven dialogue state tracking. *arXiv preprint arXiv:2310.14970* (2023).
- [15] Matthew Groh, Caleb Harris, Luis Soenksen, Felix Lau, Rachel Han, Aerin Kim, Arash Koochek, and Omar Badri. 2021. Evaluating deep neural networks trained on clinical images in dermatology with the fitzpatrick 17k dataset. In *Proceedings of the IEEE/CVF conference on computer vision and pattern recognition*. 1820–1828.
- [16] Zhaopeng Gu, Bingke Zhu, Guibo Zhu, Yingying Chen, Ming Tang, and Jinqiao Wang. 2024. Anomalygpt: Detecting industrial anomalies using large vision-language models. In *Proceedings of the AAAI conference on artificial intelligence*, Vol. 38, 1932–1940.
- [17] Xuehai He, Yichen Zhang, Luntian Mou, Eric Xing, and Pengtao Xie. 2020. Pathvqa: 30000+ questions for medical visual question answering. *arXiv preprint arXiv:2003.10286* (2020).
- [18] Yutao Hu, Tianbin Li, Quanfeng Lu, Wenqi Shao, Junjun He, Yu Qiao, and Ping Luo. 2024. OmniMedVQA: A New Large-Scale Comprehensive Evaluation Benchmark for Medical LLM. In *Proceedings of the IEEE/CVF Conference on Computer Vision and Pattern Recognition (CVPR)*. 22170–22183.
- [19] AQ Jiang, A Sablayrolles, A Mensch, C Bamford, DS Chaplot, D de Las Casas, F Bressand, G Lengyel, G Lample, L Saulnier, et al. 2023. Mistral 7b. CoRR, abs/2310.06825, 2023. doi: 10.48550. *arXiv preprint arXiv:2310.06825* (2023).
- [20] Alistair EW Johnson, Tom J Pollard, Seth J Berkowitz, Nathaniel R Greenbaum, Matthew P Lungren, Chih-ying Deng, Roger G Mark, and Steven Horng. 2019. MIMIC-CXR, a de-identified publicly available database of chest radiographs with free-text reports. *Scientific data* 6, 1 (2019), 317.
- [21] Katharina Kriegsmann, Frithjof Lobers, Christiane Zgorzelski, Joerg Kriegsmann, Charlotte Janssen, Rolf Rüdinger Meliß, Thomas Muley, Ulrich Sack, Georg Steinbuss, and Mark Kriegsmann. 2022. Deep learning for the detection of anatomical tissue structures and neoplasms of the skin on scanned histopathological tissue sections. *Frontiers in Oncology* 12 (2022), 1022967.
- [22] Jason J Lau, Soumya Gayen, Asma Ben Abacha, and Dina Demner-Fushman. 2018. A dataset of clinically generated visual questions and answers about radiology images. *Scientific data* 5, 1 (2018), 1–10.
- [23] Chunyuan Li, Cliff Wong, Sheng Zhang, Naoto Usuyama, Haotian Liu, Jianwei Yang, Tristan Naumann, Hoifung Poon, and Jianfeng Gao. 2023. Llava-med: Training a large language-and-vision assistant for biomedicine in one day. *Advances in Neural Information Processing Systems* 36 (2023), 28541–28564.
- [24] Tianbin Li, Yanzhou Su, Wei Li, Bin Fu, Zhe Chen, Ziyuan Huang, Guoan Wang, Chenglong Ma, Ying Chen, Ming Hu, et al. 2024. GMAI-VL & GMAI-VL-5.5 M: A Large Vision-Language Model and A Comprehensive Multimodal Dataset Towards General Medical AI. *arXiv preprint arXiv:2411.14522* (2024).
- [25] Weixiong Lin, Ziheng Zhao, Xiaoman Zhang, Chaoyi Wu, Ya Zhang, Yanfeng Wang, and Weidi Xie. 2023. Pmc-clip: Contrastive language-image pre-training using biomedical documents. In *International Conference on Medical Image Computing and Computer-Assisted Intervention*. Springer, 525–536.
- [26] Weixiong Lin, Ziheng Zhao, Xiaoman Zhang, Chaoyi Wu, Ya Zhang, Yanfeng Wang, and Weidi Xie. 2023. Pmc-clip: Contrastive language-image pre-training using biomedical documents. In *International Conference on Medical Image Computing and Computer-Assisted Intervention*. Springer, 525–536.
- [27] Bo Liu, Li-Ming Zhan, and Xiao-Ming Wu. 2021. Contrastive pre-training and representation distillation for medical visual question answering based on radiology images. In *Medical Image Computing and Computer Assisted Intervention–MICCAI 2021: 24th International Conference, Strasbourg, France, September 27–October 1, 2021, Proceedings, Part II* 24. Springer, 210–220.
- [28] Bo Liu, Li-Ming Zhan, Li Xu, Lin Ma, Yan Yang, and Xiao-Ming Wu. 2021. Slake: A semantically-labeled knowledge-enhanced dataset for medical visual question answering. In *2021 IEEE 18th international symposium on biomedical imaging (ISBI)*. IEEE, 1650–1654.
- [29] Bo Liu, Ke Zou, Liming Zhan, Zexin Lu, Xiaoyu Dong, Yidi Chen, Chengqiang Xie, Jiannong Cao, Xiao-Ming Wu, and Huazhu Fu. 2024. GEMeX: A Large-Scale, Groundable, and Explainable Medical VQA Benchmark for Chest X-ray Diagnosis. *arXiv preprint arXiv:2411.16778* (2024).
- [30] Gang Liu, Jinlong He, Pengfei Li, Genrong He, Zhaolin Chen, and Shenjun Zhong. 2024. PeFoMed: Parameter Efficient Fine-tuning of Multimodal Large Language Models for Medical Imaging. *arXiv preprint arXiv:2401.02797* (2024).
- [31] Haotian Liu, Chunyuan Li, Yuheng Li, and Yong Jae Lee. 2024. Improved baselines with visual instruction tuning. In *Proceedings of the IEEE/CVF Conference on Computer Vision and Pattern Recognition*. 26296–26306.
- [32] Haotian Liu, Chunyuan Li, Qingyang Wu, and Yong Jae Lee. 2023. Visual instruction tuning. *Advances in neural information processing systems* 36 (2023), 34892–34916.
- [33] Ming Y Lu, Bowen Chen, Drew FK Williamson, Richard J Chen, Melissa Zhao, Aaron K Chow, Kenji Ikemura, Ahnong Kim, Dimitra Pouli, Ankush Patel, et al. 2024. A multimodal generative AI copilot for human pathology. *Nature* 634, 8033 (2024), 466–473.
- [34] Jong Hak Moon, Hyungyung Lee, Woncheol Shin, Young-Hak Kim, and Edward Choi. 2022. Multi-modal understanding and generation for medical images and text via vision-language pre-training. *IEEE Journal of Biomedical and Health Informatics* 26, 12 (2022), 6070–6080.
- [35] Michael Moor, Qian Huang, Shirley Wu, Michihiro Yasunaga, Yash Dalmia, Jure Leskovec, Cyril Zakka, Eduardo Pontes Reis, and Pranav Rajpurkar. 2023. Med-flamingo: a multimodal medical few-shot learner. In *Machine Learning for Health (ML4H)*. PMLR, 353–367.
- [36] Binh D Nguyen, Thanh-Toan Do, Binh X Nguyen, Tuong Do, Erman Tjiputra, and Quang D Tran. 2019. Overcoming data limitation in medical visual question answering. In *Medical Image Computing and Computer Assisted Intervention–MICCAI 2019: 22nd International Conference, Shenzhen, China, October 13–17, 2019, Proceedings, Part IV* 22. Springer, 522–530.
- [37] Andre GC Pacheco, Gustavo R Lima, Amanda S Salomao, Breno Krohling, Igor P Biral, Gabriel G de Angelo, Fábio CR Alves Jr, José GM Esgario, Alana C Simora, Pedro BC Castro, et al. 2020. PAD-UFES-20: A skin lesion dataset composed of patient data and clinical images collected from smartphones. *Data in brief* 32 (2020), 106221.
- [38] Aditya Ramesh, Mikhail Pavlov, Gabriel Goh, Scott Gray, Chelsea Voss, Alec Radford, Mark Chen, and Ilya Sutskever. 2021. Zero-shot text-to-image generation. In *International conference on machine learning*. Pmlr, 8821–8831.
- [39] María Agustina Ricci Lara, María Victoria Rodríguez Kowalczyk, Maite Lisa Eliceche, María Guillermina Ferrareso, Daniel Roberto Luna, Sonia Elizabeth Benitez, and Luis Daniel Mazzuocollo. 2023. A dataset of skin lesion images collected in Argentina for the evaluation of AI tools in this population. *Scientific Data* 10, 1 (2023), 712.
- [40] Karan Singhal, Tao Tu, Juraj Gottweis, Rory Sayres, Ellery Wulczyn, Mohamed Amin, Le Hou, Kevin Clark, Stephen R Pfohl, Heather Cole-Lewis, et al. 2025.

- Toward expert-level medical question answering with large language models. *Nature Medicine* (2025), 1–8.
- [41] Ajay K Tanwani, Joelle Barral, and Daniel Freedman. 2022. Repsnet: Combining vision with language for automated medical reports. In *International Conference on Medical Image Computing and Computer-Assisted Intervention*. Springer, 714–724.
  - [42] Gemini Team, Rohan Anil, Sebastian Borgeaud, Jean-Baptiste Alayrac, Jiahui Yu, Radu Soricut, Johan Schalkwyk, Andrew M Dai, Anja Hauth, Katie Millican, et al. 2023. Gemini: a family of highly capable multimodal models. *arXiv preprint arXiv:2312.11805* (2023).
  - [43] Omkar Chakradhar Thawakar, Abdelrahman M Shaker, Sahal Shaji Mullappilly, Hisham Cholakkal, Rao Muhammad Anwer, Salman Khan, Jorma Laaksonen, and Fahad Khan. 2024. XrayGPT: Chest radiographs summarization using large medical vision-language models. In *Proceedings of the 23rd workshop on biomedical natural language processing*. 440–448.
  - [44] Omkar Thawkar, Abdelrahman Shaker, Sahal Shaji Mullappilly, Hisham Cholakkal, Rao Muhammad Anwer, Salman Khan, Jorma Laaksonen, and Fahad Shahbaz Khan. 2023. Xraygpt: Chest radiographs summarization using medical vision-language models. *arXiv preprint arXiv:2306.07971* (2023).
  - [45] Hugo Touvron, Thibaut Lavril, Gautier Izacard, Xavier Martinet, Marie-Anne Lachaux, Timothée Lacroix, Baptiste Rozière, Naman Goyal, Eric Hambro, Faisal Azhar, et al. 2023. Llama: Open and efficient foundation language models. *arXiv preprint arXiv:2302.13971* (2023).
  - [46] Philipp Tschandl, Cliff Rosendahl, and Harald Kittler. 2018. The HAM10000 dataset, a large collection of multi-source dermatoscopic images of common pigmented skin lesions. *Scientific data* 5, 1 (2018), 1–9.
  - [47] Abbi Ward, Jimmy Li, Julie Wang, Sriram Lakshminarasimhan, Ashley Carrick, Bilson Campana, Jay Hartford, Pradeep K Sreenivasaiiah, Tiya Tiyasirisokchai, Sunny Virmani, et al. 2024. Creating an Empirical Dermatology Dataset Through Crowdsourcing With Web Search Advertisements. *JAMA Network Open* 7, 11 (2024), e2446615–e2446615.
  - [48] Ruiqi Wu, Chenran Zhang, Jianle Zhang, Yi Zhou, Tao Zhou, and Huazhu Fu. 2024. MM-Retinal: Knowledge-Enhanced Foundational Pretraining with Fundus Image-Text Expertise. In *International Conference on Medical Image Computing and Computer-Assisted Intervention*. Springer, 722–732.
  - [49] Wen-wai Yim, Yajuan Fu, Zhaoyi Sun, Asma Ben Abacha, Meliha Yetisgen, and Fei Xia. 2024. Dermavqa: A multilingual visual question answering dataset for dermatology. In *International Conference on Medical Image Computing and Computer-Assisted Intervention*. Springer, 209–219.
  - [50] Hongbo Zhang, Junying Chen, Feng Jiang, Fei Yu, Zhihong Chen, Jianquan Li, Guiming Chen, Xiangbo Wu, Zhiyi Zhang, Qingying Xiao, et al. 2023. Huatuogpt, towards taming language model to be a doctor. *arXiv preprint arXiv:2305.15075* (2023).
  - [51] Sheng Zhang, Yanbo Xu, Naoto Usuyama, Jaspreet Bagga, Robert Tinn, Sam Preston, Rajesh Rao, Mu Wei, Naveen Valluri, Cliff Wong, et al. 2023. Large-scale domain-specific pretraining for biomedical vision-language processing. *arXiv preprint arXiv:2303.00915* 2, 3 (2023), 6.
  - [52] Xiaoman Zhang, Chaoyi Wu, Ziheng Zhao, Jiayu Lei, Ya Zhang, Yanfeng Wang, and Weidi Xie. 2024. Radgenome-chest ct: A grounded vision-language dataset for chest ct analysis. *arXiv preprint arXiv:2404.16754* (2024).
  - [53] Xiaoman Zhang, Chaoyi Wu, Ziheng Zhao, Weixiong Lin, Ya Zhang, Yanfeng Wang, and Weidi Xie. 2023. Pmc-vqa: Visual instruction tuning for medical visual question answering. *arXiv preprint arXiv:2305.10415* (2023).
  - [54] Xiangyu Zhao, Bo Liu, Qijiong Liu, Guangyuan Shi, and Xiao-Ming Wu. 2023. Easygen: Easing multimodal generation with bidiffuser and llms. *arXiv preprint arXiv:2310.08949* (2023).
  - [55] Lianmin Zheng, Wei-Lin Chiang, Ying Sheng, Siyuan Zhuang, Zhanghao Wu, Yonghao Zhuang, Zi Lin, Zhuohan Li, Dacheng Li, Eric Xing, et al. 2023. Judging llm-as-a-judge with mt-bench and chatbot arena. *Advances in Neural Information Processing Systems* 36 (2023), 46595–46623.
  - [56] Juexiao Zhou, Xiaonan He, Liyuan Sun, Jiannan Xu, Xiuying Chen, Yuetan Chu, Longxi Zhou, Xingyu Liao, Bin Zhang, Shawn Afvari, et al. 2024. Pre-trained multimodal large language model enhances dermatological diagnosis using SkinGPT-4. *Nature Communications* 15, 1 (2024), 5649.

# Supplementary Materials: MM-Skin: Enhancing Dermatology Vision Language Model with an Authoritative Image-Text Dataset

## A Prompt-Guided QA Generation

Recent studies like MedPLIB and LLaVA-Med have shown the effectiveness of using Large Language Models (LLMs) for generating medical VQA data. Inspired by this, we use LLMs to create a high-quality dermatology-specific VQA dataset from our image-caption pairs. The dataset, consisting of skin images and expert-written captions, is expanded using a combination of LLM-based generation and manual selection to produce 27,000 diverse, clinically relevant QA pairs. We use LLaMA-3.1 as the QA generator, employing a prompt strategy designed to encourage diverse, image-inferable questions and simulate human-AI interaction. The process is detailed in Figure 7, ensuring consistency and relevance in the generated conversations.

## B Case Study Extension

To better understand the qualitative differences between general-purpose, medical-domain, and dermatology-specific LVLMs, we compare responses from Qwen2.5-VL, LLaVA-Med, and our fine-tuned SkinVL-PubMM on selected examples from MM-Skin (Figure 8). The comparison reveals distinct patterns in each model’s reasoning ability and domain alignment.

Qwen2.5-VL, as a general-purpose model, tends to rely on prior knowledge and surface-level cues. Its answers are often vague, speculative, or overly broad, lacking grounding in the actual visual evidence. For instance, when asked about lesion progression, it speculates about potential conditions (e.g., mole, melanoma) instead of describing the lesion’s visual changes over time. This suggests that without fine-tuning, general LVLMs struggle to adapt to domain-specific visual reasoning tasks. LLaVA-Med, trained on broader medical data, shows improved familiarity with medical terminology and structure. Its responses are more medically grounded but sometimes overconfident or overly specific, potentially introducing hallucinated details not directly supported by the input. For example, its mention of “crusted and ulcerated” lesions or “high mitotic rate” reflects a tendency to default to prototypical diagnostic language, which may not be appropriate for open-ended QA grounded in image descriptions. In contrast, SkinVL-PubMM demonstrates a more balanced and context-aware approach. Fine-tuned on MM-Skin, it produces responses that are not only clinically meaningful but also better aligned with the visual descriptions available, without introducing unsupported claims. Its answer regarding tumor cells, for example, emphasizes a high nuclear-to-cytoplasmic ratio and explains its significance in plain terms—highlighting both visual specificity and interpretability. Similarly, when asked about notable image features, it identifies signs like inflammation, raised bumps, and lesion edge discoloration, offering a more complete and nuanced interpretation than the other models. Overall, these comparisons suggest that general and even medical-pretrained LVLMs lack the necessary domain grounding and sensitivity to subtle visual details in dermatology. Fine-tuning on expert-annotated, multimodal data such as MM-Skin enables models like SkinVL-PubMM

**Table 6: Training and evaluation dataset of SkinVL model**

	Dataset	Image Modality	# Train	# Test
Public Datasets	SCIN	Clinical	10407	-
	DDI	Clinical	525	133
	Fitzpatrick17k	Clinical	12772	3194
	PAD	Clinical	1839	461
	Dermnet	Clinical	-	4003
	HAM10000	Dermoscopy	-	1512
	ISIC2019	Dermoscopy	17732	7601
	BCN20000	Dermoscopy	15157	3791
	HIBA	Dermoscopy	1309	328
	MSKCC	Dermoscopy	1037	260
Ours	Patch16	Pathology	88972	28040
	MM-Skin	Clinical, Dermoscopy, Pathology	21807	5452
Total			171557	54775

to generate more accurate, grounded, and interpretable responses in skin-related VQA tasks.

## C Training and Evaluation Dataset Overview

Table 6 presents the datasets used for training and evaluation of the SkinVL model. We used 10 datasets, including 9 public datasets and our MM-Skin dataset, with testing performed on the corresponding test sets. Additional zero-shot evaluation was conducted using the Dermnet and HAM10000 test sets. The datasets cover three image modalities: Pathology (53.62%), Clinical (18.96%), and Dermoscopy (21.14%), with a similar distribution in the test set. Datasets like DDI, HIBA, and Patch16 were treated as binary classification tasks (Malignant/Non-Malignant), while others were multi-class, including ISIC (8 categories), MSKCC (21 categories), PAD (6 categories), Fitzpatrick17k (3 categories), HAM10000 (7 categories), and BCN20000 (12 categories). Dermnet, with the most categories (23), spans a range from Seborrheic Keratosis and Acne to Warts and Molluscum. These datasets ensure comprehensive evaluation.

### Prompting LLaMA to generate medical visual question and answering

```
messages = [ {"role": "system", "content": """"You are an AI assistant specialized in biomedical topics.
You are an AI assistant specialized in biomedical topics.
You are provided with a text description (Figure Caption) of a figure image from a biomedical research paper.
Unfortunately, you don't have access to the actual image.
```

Below are requirements for generating the questions and answers in the conversation:

- Avoid quoting or referring to specific facts, terms, abbreviations, dates, numbers, or names, as these may reveal the conversation is based on the text information, rather than the image itself. Focus on the visual aspects of the image that can be inferred without the text information.
- Do not use phrases like 'mentioned', 'caption', 'context' in the conversation. Instead, refer to the information as being 'in the image.'
- Ensure that questions are diverse and cover a range of visual aspects of the image.
- The conversation should include 2-4 turns of questions and answers about the visual aspects of the image.
- Answer responsibly, avoiding overconfidence, and do not provide medical advice or diagnostic information. Do not introduce any information that is not explicitl

```
]
```

```
for sample in fewshot_samples:
```

```
    messages.append({"role": "user", "content": sample['context']})
```

```
    messages.append({"role": "assistant", "content": sample['response']})
```

```
messages.append({"role": "user", "content": query})
```

**Figure 7: Illustration of the proposed pipeline for constructing MM-Skin, a dataset containing multimodal images, expert captions, demographic attributes, and QA pairs, supporting multiple downstream tasks.**

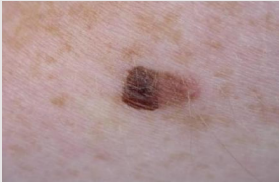
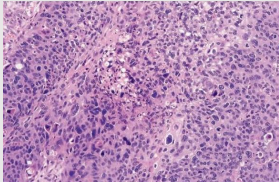

Examples from MM-Skin			
			
Q	Is there a pattern in the plaque's appearance?	Can you describe the appearance of the tumor cells?	Are there any other notable features in the image?
GT	Yes, there appears to be a <b>network-like structure</b> within the plaque. <b>This could indicate a certain type of skin condition or disease.</b>	The tumor cells appear to be <b>large</b> and <b>irregularly shaped</b> , with <b>prominent nucleoli</b> and <b>abundant cytoplasm</b> .	Yes, there appears to be some <b>inflammation</b> surrounding the vessels.
Qwen2.5-VL	The image you've provided appears to show a skin lesion, which could be indicative of various conditions such as a mole, a birthmark, or a more serious condition like melanoma. The presence of a central dark area with a lighter border is often characteristic of a mole, <b>but it's important to note that this alone does not diagnose any condition.</b>	The image appears to be a histological section stained with hematoxylin and eosin (H&E), which is commonly used in pathology to visualize tissue structures. <b>(no detail)</b>	The image appears to show a close-up of skin with visible red, thread-like structures that could be interpreted as spider veins or telangiectasias. These are small blood vessels that have become dilated and visible on the surface of the skin. There are no other notable features in the image that stand out; it is primarily focused on these vascular structures.
LLaVA-Med	Yes, the plaque appears to have a "targetoid" pattern. This pattern is characterized by a central area of hyperpigmentation surrounded by a lighter, hypopigmented area.	The tumor cells in the image appear to be <b>large</b> , with <b>abundant eosinophilic cytoplasm</b> . They are arranged in nests and cords, and they have a high mitotic rate, which means they are dividing rapidly.	Yes, there are other notable features in the image. These include hyperpigmentation, which is an increase in the amount of melanin in the skin, and a few hypopigmented areas, which are regions with less melanin than the surrounding skin.
SkinVL-PubMM	Yes, the plaque has a reticulate pattern, which means it has a <b>network-like appearance</b> .	The tumor cells appear to be <b>large</b> and <b>irregularly shaped</b> , with a <b>high nuclear-to-cytoplasmic ratio</b> . This means that the nuclei of the cells are relatively large compared to the amount of cytoplasm, which is the material surrounding the nucleus.	Yes, there are several other notable features in the image. One is the presence of multiple small, raised bumps on the skin, which could indicate <b>inflammation or infection</b> . Additionally, there appears to be some discoloration around the edges of the lesions, suggesting possible scarring or damage to the surrounding tissue.

Figure 8: Example questions from MM-Skin answered by Qwen2.5-VL, and LLaVA-Med our fine-tuned SkinVL-PubMM. These examples highlight the limitations of LVLMs like Qwen2.5-VL in visual reasoning, which can be effectively improved by fine-tuning with MM-Skin dataset.